Longitudinal convection rolls in a rectangular channel heated from below

Kato, Yuki
Department of Applied Mathematics and Physics, Tottori University

Fujimura, Kaoru
Department of Applied Mathematics and Physics, Tottori University

https://doi.org/10.15017/27085

出版情報：九州大学応用力学研究所所報. 139, pp.43-55, 2010-09. Research Institute for Applied Mechanics, Kyushu University
バージョン：
権利関係：

Longitudinal convection rolls in a rectangular channel heated from below

Yuki KATO*1and Kaoru FUJIMURA*1
E-mail of corresponding author: *kato@damp.tottori-u.ac.jp*

(Received July 30, 2010)

Abstract

The sidewall effect on Rayleigh-Bénard convection has been examined in a rectangular channel of infinite length having a cross section with a finite aspect ratio A (=width/height). Steady longitudinal rolls are obtained numerically. In a bifurcation diagram in which A is changed as a bifurcation parameter, the roll solution forms a single-valued branch when the Rayleigh number Ra exceeds but is still close to the critical value. When Ra is relatively higher, the solution branch has a folded structure, that is, it can be triple-valued. The secondary instability of the roll solution with respect to two-dimensional disturbances is investigated. The roll solutions with a certain symmetry are found to be linearly stable. Stable roll patterns are classified in the A-Ra plane. In a certain range of A and Ra, multiple roll patterns are simultaneously stable. The number of the stable patterns increases with Ra.

Key words : *steady thermal convection, longitudinal rolls, rectangular channel, secondary instability, avoided crossing.*

1. Introduction

In Rayleigh-Bénard problem with a superimposed through-flow, a variety of convection patterns are observed depending on the thermal stratification and through-flow.[1,2] When the Poiseuille flow is imposed on the thermal convection in a horizontally infinite layer, thermal convection rolls are realized for the Rayleigh number Ra above the critical value (= 1708) and the Reynolds number Re below the critical value (= 5490).[3,4] At the onset of the convection, rolls are aligned along the streamwise direction. We call such convection rolls *longitudinal*. For industrial applications such as chemical engineering processes, we often cannot neglect sidewall effects on the convection pattern. In a rectangular channel with rigid sidewalls, the thermal convection pattern changes with the Reynolds number of the through-flow. According to a linear stability analysis for sufficiently low Re, the primary pattern is a transverse mode which is periodic in the streamwise direction.[5] For Re above a threshold value, the primary pattern is longitudinal. Although the longitudinal rolls in the rectangular channel are similar to the rolls in the infinite layer, sidewalls affect details of the roll pattern. The number of rolls and their arrangement at the onset are known to depend on the aspect ratio A(=width/height) of the cross section of the channel. We here focus on the longitudinal roll patterns in the rectangular channel that are realized when Re is above the threshold. By determining longitudinal roll pattern as a function of A, we aim to reveal sidewall effects on the roll patterns.

We briefly review a sidewall effect on the onset of the longitudinal rolls. The fully developed longitudinal rolls are essentially two-dimensional and do not depend on the through-flow, as will be explained in §2. The stability of the conduction state with respect to the longitudinal rolls is therefore governed by the two-dimensional problem. The stability in the two-dimensional box has been examined by many authors.[6-14] The neutral Rayleigh numbers are obtained as functions of the aspect ratio A, as shown in Fig. 1. Among the several neutral Rayleigh numbers, the lowest for a prescribed aspect ratio is the critical Rayleigh number. When A is close to an integer n, the convection pattern at the onset consists of n rolls aligned horizontally. We note that some neutral curves cross in the A-Ra plane. We can see the crossing between the curve for an odd number of rolls (the solid line in Fig. 1) and the curve for an even number of rolls (the dashed line). On the other hand, the two curves for an odd number of rolls *avoid crossing*; similarly the two curves for an even number of rolls also avoid crossing.[9,15,16] The avoided crossing of the neutral curves is one of the remarkable sidewall

*1 Department of Applied Mathematics and Physics, Tottori University

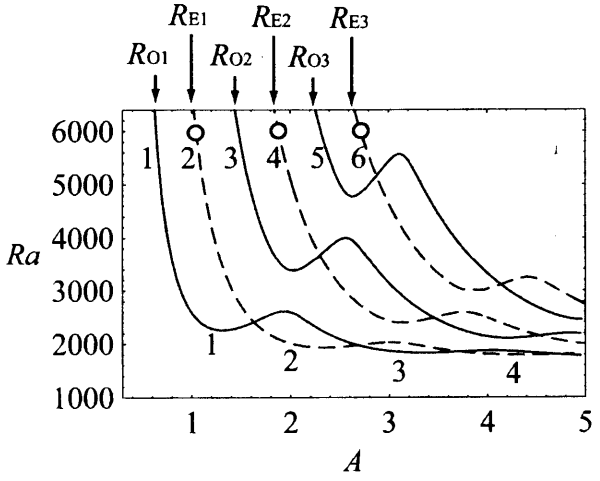

Fig. 1 Linear neutral stability curves for longitudinal convection rolls. Perfectly insulating sidewall. The curves are based on the first six eigenvalues. The numbers in the figure indicate the number of rolls. We name the first, second and third curves for the odd number of rolls R_{O1}, R_{O2} and R_{O3}, respectively. We name the curves for even rolls, R_{E1}, R_{E2} and R_{E3}, similarly. Two neutral curves, one for an odd number of rolls (solid lines) and one for an even number of rolls (dashed lines), cross. Two curves for the same symmetry avoid crossing. For open circles, see Fig. 3.

effects provided by rigid sidewalls.

A crossing of the neutral curves gives rise to a nonlinear interaction of two modes, n rolls and $n+1$ rolls. The interaction yields a mixed mode of n rolls and $n+1$ rolls.[17-20] Mizushima and Adachi obtained one roll, two rolls, and a mixed mode of them in a square box with perfectly conducting sidewalls.[21] They studied a bifurcation of the roll solutions in detail at $A = 1$ and $0 < Ra < 70000$. They found that both the one-roll solution and two-roll solution are stable simultaneously when $16624 < Ra < 37046$.

When the neutral curves avoid crossing, its influence on a nonlinear solution has not yet been completely resolved. Recently, we demonstrated that the avoided crossing affects a secondary bifurcation of a mixed mode of n rolls and $n+2$ rolls, based on a weakly nonlinear analysis as well as a numerical analysis.[22,23] At some selected values of Ra, solution branches were obtained as functions of the aspect ratio A. The branches are folded in a parameter space. They connect multiple stable solutions. A branch connects, for instance, a stable two-roll solution and a stable four-roll solution via an unstable solution. This bifurcation structure can be explained based on amplitude equations:

$$\frac{da}{dt} = \lambda_1 a + \epsilon_1 b + \mu_1 a^3 + \mu_2 b^2 a, \tag{1a}$$

$$\frac{db}{dt} = \epsilon_2 a + \lambda_2 b + \mu_3 a^2 b + \mu_4 b^3, \tag{1b}$$

where a and b denote amplitudes of n rolls and $n+2$ rolls, respectively. Two linear terms $\epsilon_1 b$ and $\epsilon_2 a$ represent the influence of the avoided crossing.

In the present paper, we extend the numerical results in refs. 22 and 23 in order to reveal a comprehensive bifurcation structure of the longitudinal rolls including stability characteristics in a wide range of A and Ra. In the numerical analysis in refs. 22 and 23, roll solutions were limited to even number of rolls for the perfectly insulating sidewalls; in addition their stability was examined only with respect to the disturbance that has an even symmetry. In this study, we investigate bifurcation of roll solutions, which include even number of rolls, odd number of rolls, and the mixed mode of them for perfectly conducting sidewalls as well as insulating one. We examine the secondary instability of the roll solutions with respect to two-dimensional disturbance without any assumptions on its symmetry.

We mention another systems where multiple rolls on a folded branch were found. They are Taylor-Couette flow between two cylinders of finite length[24-27] and a thermal convection in a rectangular channel with imperfect boundary conditions.[28] In the latter system, the top half of the sidewalls is assumed to be insulating and the bottom half is maintained at a uniform temperature. In both systems, the primary bifurcation is imperfect; there is no critical Taylor number or Rayleigh number of an onset of convection rolls. The folded branch is due to the imperfection of the primary bifurcation. The effect of the imperfection was studied based on the following equations:

$$\frac{da}{dt} = \lambda_1 a + \mu_1 a^3 + \mu_2 b^2 a + \delta_1, \tag{2a}$$

$$\frac{db}{dt} = \lambda_2 b + \mu_3 a^2 b + \mu_4 b^3 + \delta_2. \tag{2b}$$

Here, the last terms δ_1 and δ_2 are constants that give rise to the imperfect primary bifurcation.[26,27] In our study, we assume that the sidewalls are perfectly conducting or perfectly insulating. The primary bifurcation is then perfect, which is in contrast to the imperfect bifurcation in the Taylor-Couette flow in refs. 24–27 or the thermal convection in ref. 28.

We explain the mathematical formulation and symmetry of the convection rolls in §2, and the numerical methods in §3. In §4, we first explain the folded solution branches of primary convection rolls under particular symmetries. We then show asymmetric patterns. In §5, we classify stable roll patterns in the A-Ra plane

and predict roll patterns achieved in laboratory experiments.

2. Formulation

2.1 Basic equations

Under the Boussinesq approximation, we consider a fluid motion in a rectangular channel with horizontal top and bottom walls located at $z^* = \pm h/2$ and vertical sidewalls located at $x^* = \pm d/2$. We define the aspect ratio of the cross section as $A = d/h$. The channel is heated from below and cooled from above at different, but uniform, temperatures $T^* = T_0 \mp \Delta T/2$ at $z^* = \pm h/2$, where T_0 is a reference temperature measured at $z^* = 0$ and $\Delta T(> 0)$ is the temperature difference between the top and bottom walls. The temperature in the conduction state is $T^* = \Theta^*(z^*) \equiv T_0 - \Delta T z^*/h$. We use the height of the channel h, the thermal diffusive time h^2/κ, and the temperature difference ΔT as the characteristic length, time, and temperature, respectively. Here, κ is the thermal diffusivity. We introduce non-dimensional variables. We denote them by letters without an asterisk.

We impose a steady and fully developed through-flow. We assume that the channel has an infinite length. We consider a fully developed state both thermally and hydrodynamically. We define the Reynolds number Re, based on a half of the height of the channel and the maximum velocity of the through-flow. When Re exceeds a certain threshold, Re_*, the longitudinal rolls are achieved. Here, Re_* is $O(10)$ for air, and $A = 1 - 5.2$.[5,29,30]

We consider fully developed longitudinal rolls for $Re > Re_*$. The velocity for the fully developed rolls is uniform in the streamwise direction. We can therefore introduce a stream function ψ in the x-z plane such that the spanwise velocity u and the vertical velocity w are related to ψ by $\psi_z = u$ and $\psi_x = -w$, where the subscripts denote partial derivatives. We introduce a temperature deviation from the conduction state by $\theta = T - \Theta$. The stream function ψ and the temperature disturbance θ in the fully developed longitudinal rolls are independent of the through-flow. They therefore satisfy equations of two-dimensional form:

$$\frac{\partial}{\partial t}\nabla^2\psi = Pr\nabla^4\psi - PrRa\frac{\partial\theta}{\partial x} + J(\psi, \nabla^2\psi), \tag{3a}$$

$$\frac{\partial\theta}{\partial t} = \nabla^2\theta - \frac{\partial\psi}{\partial x} + J(\psi, \theta). \tag{3b}$$

Here, $\nabla^2 = \partial_{xx} + \partial_{zz}$ is the two-dimensional Laplacian, and J is the Jacobian $J(f, g) = f_x g_z - f_z g_x$. The Prandtl number Pr and the Rayleigh number Ra are defined by $Pr = \nu/\kappa$ and $Ra = \alpha g(\Delta T)h^3/(\nu\kappa)$, respectively. Here, ν is the kinematic viscosity, α is the coefficient of cubic expansion, and g is the gravitational acceleration. We let the Prandtl number be $Pr = 0.71$ by assuming that the working fluid is air.

We impose boundary conditions on the stream function:

$$\psi = \frac{\partial\psi}{\partial x} = 0 \quad \text{at} \quad x = \pm A/2, \tag{4a}$$

$$\psi = \frac{\partial\psi}{\partial z} = 0 \quad \text{at} \quad z = \pm 1/2. \tag{4b}$$

On the temperature disturbance, we impose the perfectly conducting boundary conditions on the top and bottom walls:

$$\theta = 0 \quad \text{at} \quad z = \pm 1/2. \tag{5}$$

On the sidewalls, we impose the following perfectly conducting boundary conditions:

$$\theta = 0 \quad \text{at} \quad x = \pm A/2, \tag{6}$$

or the following perfectly insulating conditions:

$$\frac{\partial\theta}{\partial x} = 0 \quad \text{at} \quad x = \pm A/2. \tag{7}$$

Equations (3) are equivalent to the governing equations of the convection in a two-dimensional box heated from below. For $A = 1$, eqs. (3) with boundary conditions (4), (5) and (6) have been extensively investigated by Mizushima and Adachi.[21]

2.2 Steady solution and the Nusselt number

The longitudinal rolls are steady solutions of (3). We denote the steady solutions by $\overline{\psi}(x, z)$ and $\overline{\theta}(x, z)$. They satisfy

$$\nabla^4\overline{\psi} - Ra\frac{\partial\overline{\theta}}{\partial x} = -\frac{1}{Pr}J(\overline{\psi}, \nabla^2\overline{\psi}), \tag{8a}$$

$$\nabla^2\overline{\theta} - \frac{\partial\overline{\psi}}{\partial x} = -J(\overline{\psi}, \overline{\theta}) \tag{8b}$$

with boundary conditions (4), (5), and (6) [or (7)].

According to the linear stability analysis of the conduction state, n rolls at the onset are aligned horizontally when A is close to an integer n.[8] Based on the linearized equations of (3), if n is odd, then the temperature $\overline{\theta}(x, z)$ of the n-roll mode is an odd function of x and an even function of z; the stream function $\overline{\psi}(x, z)$ is an even function of both x and z. When we take the right-hand side of (8) into account, the nonlinear interaction of this odd-roll mode with itself results in nonlinear solutions satisfying

$$\mathrm{O}_1: \quad \overline{\psi}(-x, -z) = \overline{\psi}(x, z) \quad \text{and} \quad \overline{\theta}(-x, -z) = -\overline{\theta}(x, z). \tag{9}$$

We herein refer to a steady solution with the above symmetry (9) as an *odd solution*. At given values of Ra, A

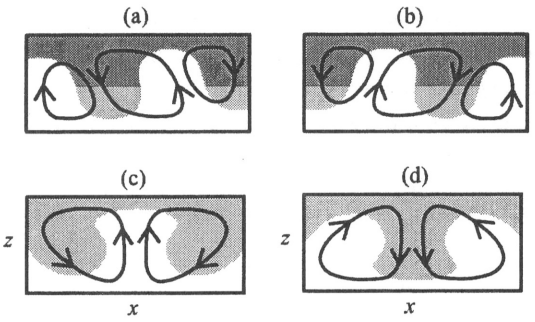

Fig. 2 Sketches of stream lines and temperature fields of odd solutions [(a), (b)] and even solutions [(c), (d)]. Gray and white regions represent relatively hotter and colder regions, respectively.

and Pr, we have two odd solutions simultaneously. Suppose that we obtain one odd solution; a transformation

$$z \to -z, \qquad \phi \to -\phi, \qquad \theta \to -\theta \tag{10}$$

yields the other odd solution. An example of a couple of odd solutions is shown in Fig. 2 (a), (b).

When n is even, the temperature $\overline{\theta}(x,z)$ of the linear n-roll mode is an even function of both x and z. The corresponding nonlinear solution satisfies

$$\mathrm{E}_2: \quad \overline{\psi}(-x,z) = -\overline{\psi}(x,z) \quad \text{and} \quad \overline{\theta}(-x,z) = \overline{\theta}(x,z). \tag{11}$$

We refer to a steady solution with the symmetry (11) as an *even solution*. We show a sketch of the even solution in Fig. 2 (c). Transforming the flow pattern shown in Fig. 2 (c) by (10), we have the other pattern shown in Fig. 2 (d). We thus have two even solutions at given values of Ra, A and Pr.

In addition to the odd or even solution, there exists another class of steady solution, i.e., one which does not have any symmetry. This class arises by the secondary bifurcation from the odd or even solutions, as will be explained later. We refer to this as an *asymmetric solution*.

As a measure of the intensity of the steady rolls, we adopt the Nusselt number Nu that characterizes the vertical heat transfer due to the thermal convection. We define the Nusselt number on the top and bottom walls as

$$Nu_{\pm}(x) = -\frac{\partial T}{\partial z}(x, \pm 1/2) = 1 - \frac{\partial \overline{\theta}}{\partial z}(x, \pm 1/2). \tag{12}$$

The conduction state gives $Nu_{\pm}(x) = 1$. The mean values of the Nusselt numbers on the top and bottom walls are defined as

$$\overline{Nu}_{\pm} = \frac{1}{A}\int_{-A/2}^{A/2} Nu_{\pm}(x)\mathrm{d}x. \tag{13}$$

We denote the mean value of $\overline{Nu}_+$ and $\overline{Nu}_-$ as $\overline{Nu}$.

Note that the dependence of the Nusselt number on the aspect ratio is practically important. Nicolas pointed out that the sidewall effect on the heat transfer by the fully developed rolls had not been investigated thoroughly.[2] The question as to whether Nu increases as A increases remains to be answered.

2.3 Secondary instability of longitudinal rolls

In order to examine the secondary instability of the longitudinal rolls, we add infinitesimal disturbances to the solutions of (8): $\psi = \overline{\psi} + \hat{\psi}\exp(\sigma t)$ and $\theta = \overline{\theta} + \hat{\theta}\exp(\sigma t)$. Here, the variables with a hat denote the amplitude of the infinitesimal disturbance; the amplitude depends on x and z only. Substituting these into (3) and linearizing with respect to the disturbance, we obtain

$$\sigma\nabla^2\hat{\psi} = Pr\nabla^4\hat{\psi} - PrRa\frac{\partial\hat{\theta}}{\partial x} + J(\overline{\psi}, \nabla^2\hat{\psi}) + J(\hat{\psi}, \nabla^2\overline{\psi}), \tag{14a}$$

$$\sigma\hat{\theta} = \nabla^2\hat{\theta} - \frac{\partial\hat{\psi}}{\partial x} + J(\overline{\psi}, \hat{\theta}) + J(\hat{\psi}, \overline{\theta}). \tag{14b}$$

The disturbance satisfies the boundary conditions (4)–(7). Equations (14) with boundary conditions constitute an eigenvalue problem with eigenvalue σ and corresponding eigenfunction $(\hat{\psi}, \hat{\theta})$.

When the steady solution $(\overline{\psi}, \overline{\theta})$ has the odd symmetry, the disturbance is classified into two types. One type satisfies the same symmetry as the steady solution's, that is, the symmetry O_1 [see eq. (9)]. The second type satisfies an counterpart of the symmetry O_1, that is,

$$\mathrm{E}_1: \quad \hat{\psi}(-x,-z) = -\hat{\psi}(x,z) \quad \text{and} \quad \hat{\theta}(-x,-z) = \hat{\theta}(x,z). \tag{15}$$

Similarly, when the steady solution is even, the disturbance satisfies the symmetry E_2 [eq. (11)] or

$$\mathrm{O}_2: \quad \hat{\psi}(-x,z) = \hat{\psi}(x,z) \quad \text{and} \quad \hat{\theta}(-x,z) = -\hat{\theta}(x,z). \tag{16}$$

If the z dependence is neglected, then the symmetry E_1 has the same property as E_2 with respect to the reflection $x \to -x$. In this sense, a disturbance satisfying E_1 represents a similar pattern to the even rolls satisfying E_2. In the same sense, the disturbance with the symmetry O_2 is similar to the odd rolls satisfying O_1. We herein refer to a disturbance satisfying E_i or O_i $(i = 1, 2)$ shortly as a disturbance E_i or O_i, respectively.

To examine the stability of the even solution in refs. 22 and 23, we have assumed the disturbance E_2 only. In the present paper, we do not impose any restriction on the symmetry of disturbance. It is important to consider the disturbance O_2 on the even solution

and the disturbance E_1 on the odd solution, since such disturbances determine stability boundary of the roll solution as will be explained in §4.

3. Numerical method

To solve (8) and (14), we use a Chebyshev collocation method. We expand the stream function and temperature of the longitudinal rolls as

$$\overline{\psi}(x,z)=\sum_{m=0}^{M}\sum_{n=0}^{N}\psi_{mn}F_m(\xi)F_n(\zeta), \tag{17a}$$

$$\overline{\theta}(x,z)=\begin{cases}\displaystyle\sum_{m=0}^{M}\sum_{n=0}^{N}\theta_{mn}G_m(\xi)G_n(\zeta),\\ \quad\text{for perfectly conducting conditions,}\\ \displaystyle\sum_{m=0}^{M}\sum_{n=0}^{N}\theta_{mn}H_m(\xi)G_n(\zeta),\\ \quad\text{for perfectly insulating conditions,}\end{cases} \tag{17b}$$

where $\xi = 2x/A$ and $\zeta = 2z$. The functions $F_n(x)$, $G_n(x)$ and $H_n(x)$ are defined as

$$\begin{aligned}
F_{2n}(x) &= T_{2n+4}(x) - (n+2)^2T_2(x)\\
&\quad +(n+1)(n+3)T_0(x),\\
F_{2n+1}(x) &= T_{2n+5}(x) - \frac{1}{2}(n+2)(n+3)T_3(x)\\
&\quad +\frac{1}{2}(n+1)(n+4)T_1(x),\\
G_{2n}(x) &= T_{2n+2}(x) - T_0(x),\\
G_{2n+1}(x) &= T_{2n+3}(x) - T_1(x),\\
H_0(x) &= T_0(x),\\
H_{2n}(x) &= T_{2n+2}(x) - (n+1)^2T_2(x), \quad \text{for} \quad n\neq 0,\\
H_{2n+1}(x) &= T_{2n+3}(x) - (2n+3)^2T_1(x),
\end{aligned}$$

where $T_n(x)$ is the Chebyshev polynomial of degree n. The functions F_n, G_n, and H_n satisfy the boundary conditions $F_n(\pm1) = F_n'(\pm1) = G_n(\pm1) = H_n'(\pm1) = 0$, so that (17) satisfy the boundary conditions (4)–(7).

Substituting (17) into (8) and evaluating the resultant equations at collocation points, we obtain algebraic equations for $2(M+1)(N+1)$ coefficients ψ_{mn} and θ_{mn}. We solve these algebraic equations by the Newton-Raphson iteration with a continuation method using a pseudo-arclength.[31] As the collocation points, we adopt points giving the extrema of the Chebyshev polynomial of degrees $N+2$ and $M+2$. The functions F_n, G_n and H_n are even (or odd) functions when n is even (or odd). Therefore, in steady solutions with symmetries O_1 or E_2, a half of the $2(M+1)(N+1)$ coefficients are exactly zero.

When we solve (8), we mainly use $M = 84$ and $N = 24$. When the number of rolls is less than five, we also use $M = 44$ and $N = 24$. We estimate the error of the Nusselt number for an eight-roll solution at $A = 8$ and $Ra = 10000$ by increasing M or N. The relative error of the local Nusselt number $Nu_{\pm}(x)$ was less than 0.7%. The maximum error was found near $x = 0$, where the collocation points are sparse.

When we examine the linear stability of the steady solution, we expand the amplitudes of the disturbance $\hat{\psi}$ and $\hat{\theta}$ as (17). We apply the same procedure as above to eq. (14) and obtain an algebraic eigenvalue problem, which is solved using the dgegv package in LAPACK.

4. Folded branches and mixed mode solutions at a fixed value of Ra

In this section, we consider solutions at $Ra = 6000$. Longitudinal roll solutions are classified into three categories: even solutions satisfying E_2, odd solutions satisfying O_1, and asymmetric solutions. First, we focus on even solutions to explain folded branches. The bifurcation characteristics of the odd solutions are similar to those of the even solutions. Next, we show the asymmetric solutions that connect even and odd solutions. In this section, we mainly explain the solutions for perfectly insulating sidewalls. In the case of perfectly conducting sidewalls, the bifurcation structure remains unchanged qualitatively.

The roll solutions bifurcate from the solution corresponding to the conduction state. Figure 1 shows the neutral stability curves of the conduction state with respect to the rolls. The bifurcation points for the even roll solutions are located on the neutral curves for even rolls, R_{E1}, R_{E2}, and R_{E3} (shown by the dashed lines in Fig. 1). At $Ra = 6000$, the first, second and third bifurcation points are $A = 1.04$, 1.88 and 2.72, respectively, for the perfectly insulating condition. Figure 3 shows the first, second and third solution branches which bifurcate at the first, second and third bifurcation points, respectively. The three bifurcation points are located on $\overline{Nu} = 1$ in Fig. 3. We note that points at which the branches intersect with $\overline{Nu} > 1$ are not bifurcation points.

Each branch shown in Fig. 3 is folded with several loops. The folds are linked with the avoided crossing of the linear neutral curves.[22,23] Along the loop of the first branch, a convection pattern changes from n rolls to $n+2$ rolls. We show the patterns along the loop connecting two rolls and four rolls in Fig. 4. The change in the pattern from two rolls to four rolls is gradual along the branch. Roll patterns change gradually along the second and third solution branches, too. The patterns on the second and third branches are less regular; each roll has a quite different size (not shown in the figures).

Here, we remark on multiplicity of the solution. Two even solutions, which are transformed by (10) each other, give the same value of $\overline{Nu}$; we cannot distinguish

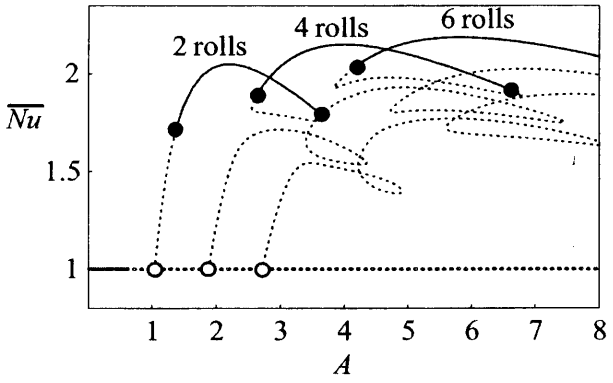

Fig. 3 The Nusselt number for the even solutions at $Ra = 6000$. Perfectly insulating sidewalls. $Pr = 0.71$. The solid lines denote linearly stable solutions, and the dotted lines denote unstable solutions. The line $\overline{Nu} = 1$ represents the conduction state. The open circles denote the bifurcation points, which correspond to the circles in Fig. 1. Dots denote bifurcation points at which the asymmetric solutions bifurcate (see Fig. 6).

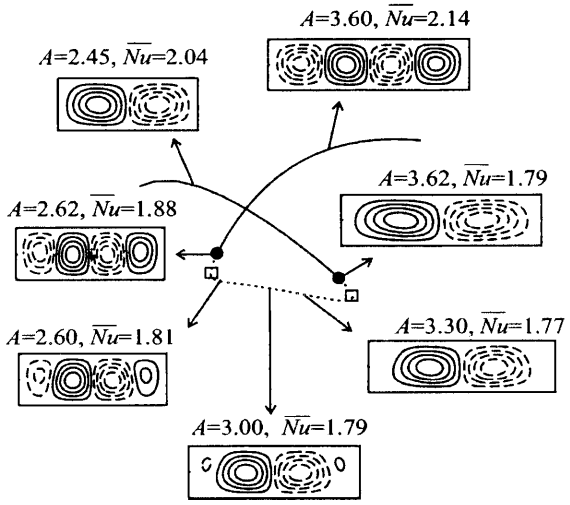

Fig. 4 Convection patterns along the first branch in Fig. 3. The solid and dashed contours denote stream lines with negative and positive values of ψ, respectively. Perfectly insulating sidewalls. For dots and squares, see Fig. 5.

two solutions in the A-$\overline{Nu}$ plane. The single branch of the even solution in the A-$\overline{Nu}$ plane thus represents double-valued solutions.

We study the secondary instability of the roll solutions by solving the eigenvalue problem (14). The stability analysis reveals that the second and third solutions are unstable. The stability of the first solution changes along the branch. We denote the growth rates

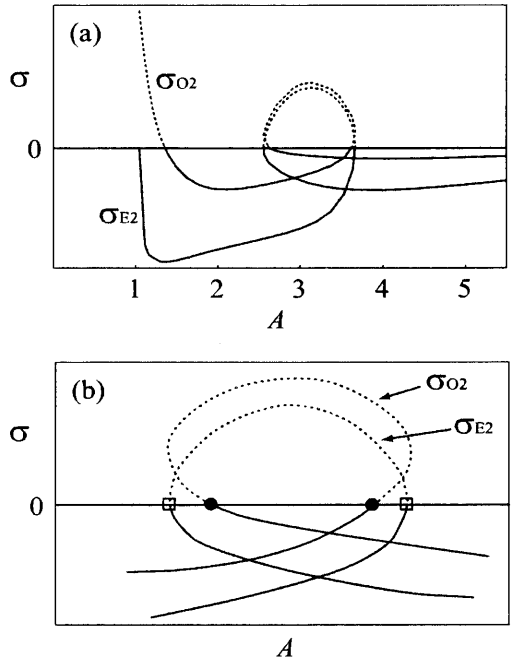

Fig. 5 Growth rates of disturbances satisfying (11) and (16). (a): σ_{E2} and σ_{O2} for the first even solution at $Ra = 6000$. Perfectly insulating sidewalls. (b): A sketch of σ_{E2} and σ_{O2} for $2 < A < 4$. The solid and dotted lines correspond to negative or positive value of σ, respectively. The squares denote saddle-node points with $\sigma_{E2} = 0$ and the dots denote the points with $\sigma_{O2} = 0$; they correspond to symbols in Fig. 4.

of the disturbances E_2 and O_2 by σ_{E2} and σ_{O2}, respectively. Here, the growth rates are given by the eigenvalues whose real part is the largest under the symmetry E_2 or O_2. Along the first branch, both σ_{E2} and σ_{O2} were real. Figure 5 shows σ_{E2} and σ_{O2} along the loop shown in Fig. 4. The growth rate σ_{E2} changes its sign at saddle-node points in the loop; it is positive only in a segment between two saddle-node points. A segment of the solution branch where $\sigma_{O2} > 0$ is slightly longer than the segment where $\sigma_{E2} > 0$. We show the points at which $\sigma_{O2} = 0$ by dots in Figs. 3, 4 and 5(b); they are always located on the segment where $\sigma_{E2} < 0$. That is, the even solution loses its stability with respect to the disturbance O_2. The points at which $\sigma_{O2} = 0$ are bifurcation points from the even solution to an asymmetric solution.

The bifurcation characteristics of the odd solution are qualitatively similar to those of the even solution. The first, second and third solution branches are folded with loops. The second and third solutions are unstable. The first solution changes its stability along the branch in a similar manner to one in Fig. 5. At points with the first eigenvalue $\sigma = 0$, the first odd solution

loses its stability with respect to the disturbance E_1. These points are secondary bifurcation points at which an asymmetric solution bifurcates. The only difference between odd and even solutions is a stability around the primary bifurcation points on $\overline{Nu} = 1$. The two-roll solution bifurcates from the conduction state at $A = 1.04$ for $Ra = 6000$; it is unstable when $1.04 < A < 1.2$ (see Fig. 3). The one-roll solution bifurcates at $A = 0.64$ for $Ra = 6000$; the one-roll solution is stable when $0.64 < A < 2.0$.

As explained above, when an even (or odd) solution loses its stability, the disturbance O_2 (or E_1) grows. As a result, an asymmetric solution bifurcates. Figure 6 shows the even and odd solution branches (the primary branches) and the asymmetric solution branches (the secondary branches). The asymmetric solution branches connect the even and odd solutions. In Fig. 6(a), we show two asymmetric branches. The left branch connects one roll and two rolls, and the right branch connects three rolls and four rolls. Figure 6(b) shows another two asymmetric branches. The left branch connects two rolls and three rolls, and the right branch connects four rolls and five rolls.

Figure 7 shows an example of the convection patterns on the left branch in Fig. 6(b). The asymmetric solutions connect two rolls that are elongated horizontally with three rolls that are elongated vertically in a tight box. Note that all of the asymmetric solutions are unstable as far as we examined.

Here, we remark on multiplicity of solutions, again. As mentioned earlier, there are two even solutions that give the same value of $\overline{Nu}$; each of them is transformed to the other by (10). From one of two even solutions, two asymmetric solutions arise out of the pitchfork bifurcation. We show a corresponding change in flow pattern in Fig. 8. For instance, from a pattern of two rolls shown in Fig. 8 (c), two kinds of asymmetric patterns arise, which are shown in Fig. 8 (e-1) and (e-3). Similarly, from the other two-roll pattern [Fig. 8 (d)], two kinds of asymmetric patterns [Fig. 8 (e-2), (e-4)] arise. We therefore have four asymmetric patterns that give the same value of $\overline{Nu}$. A bifurcation from the odd solution to asymmetric solutions is also pitchfork. From a pattern of three rolls in Fig. 8 (a), two kinds of asymmetric patterns [Fig. 8 (e-1), (e-2)] arise; from the other pattern in Fig. 8 (b), two patterns [Fig. 8 (e-3), (e-3)] arise. The single branch of the asymmetric solution in the A-$\overline{Nu}$ plane thus represents fourth-valued solutions.

5. Diagram of stable solutions

Hereafter, we focus on the first even solution and the first odd solution. The other solutions, such as the asymmetric solutions, are unstable as mentioned in the previous section.

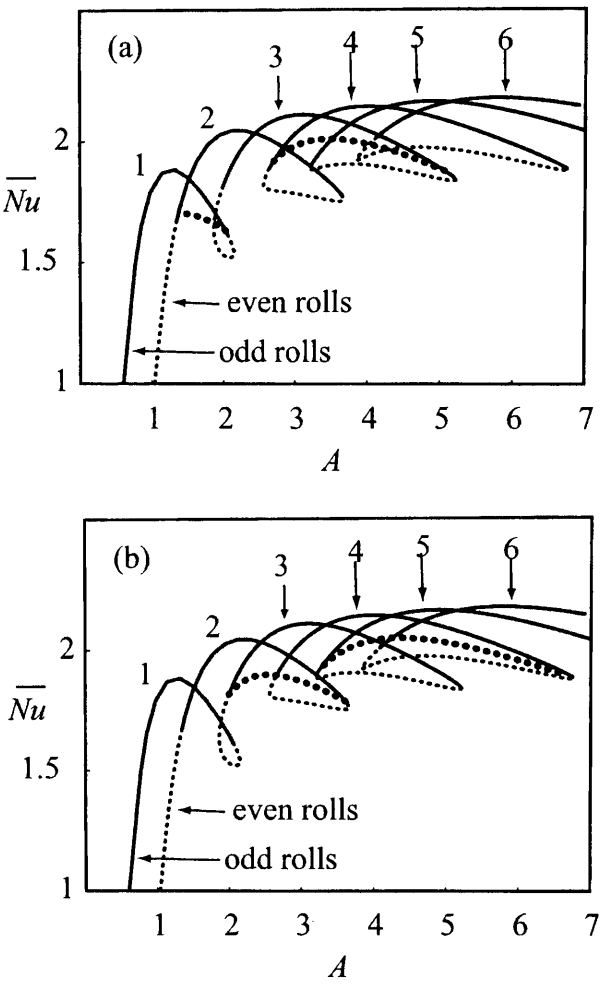

Fig. 6 Branches of the first even solution, the first odd solution, and the asymmetric solutions at $Ra = 6000$. Perfectly insulating sidewalls. The asymmetric solutions connect n rolls and $n+1$ rolls; $n = 1, 3$ in (a) and $n = 2, 4$ in (b). The even and odd solutions in (b) are the same as in (a). The solid lines denote linearly stable solutions and the dotted lines denote unstable ones. The thick dotted lines denote the asymmetric solutions, which are unstable. The numbers in the figures represent the numbers of rolls.

We explain even solutions and odd solutions separately for a while for convenience' sake. Figures 9 (a) and (b) show the even and odd solution branches, respectively, at several values of Ra. Depending on A and Ra, $\overline{Nu}(A)$ is single-valued or multi-valued. When Ra is close to the neutral value R_{E1} or R_{O1}, $\overline{Nu}(A)$ is smooth and single-valued. For instance, we see the single-valued curve for $Ra = 3000$ and $A < 3.9$ in Fig. 9(b). As Ra increases, a cusp appears on the branch at a certain value of Ra (R_{cusp}, say). Above $Ra = R_{cusp}$, $\overline{Nu}(A)$ is

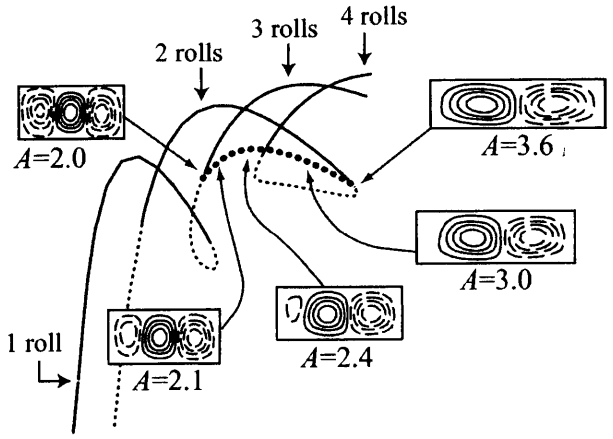

Fig. 7 Convection patterns of the asymmetric solution connecting two rolls and three rolls in Fig. 6(b). $Ra = 6000$. Perfectly insulating sidewalls.

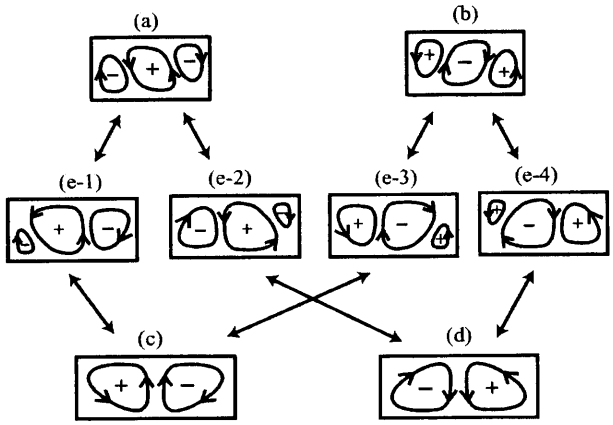

Fig. 8 Sketches of stream lines of odd solutions [(a), (b)], even solutions [(c), (d)] and asymmetric solutions connecting them [(e-1), (e-2), (e-3), (e-4)]. Plus and minus signs denote direction of rotation for a reference. (a)-(d) correspond to the labels in Fig. 2.

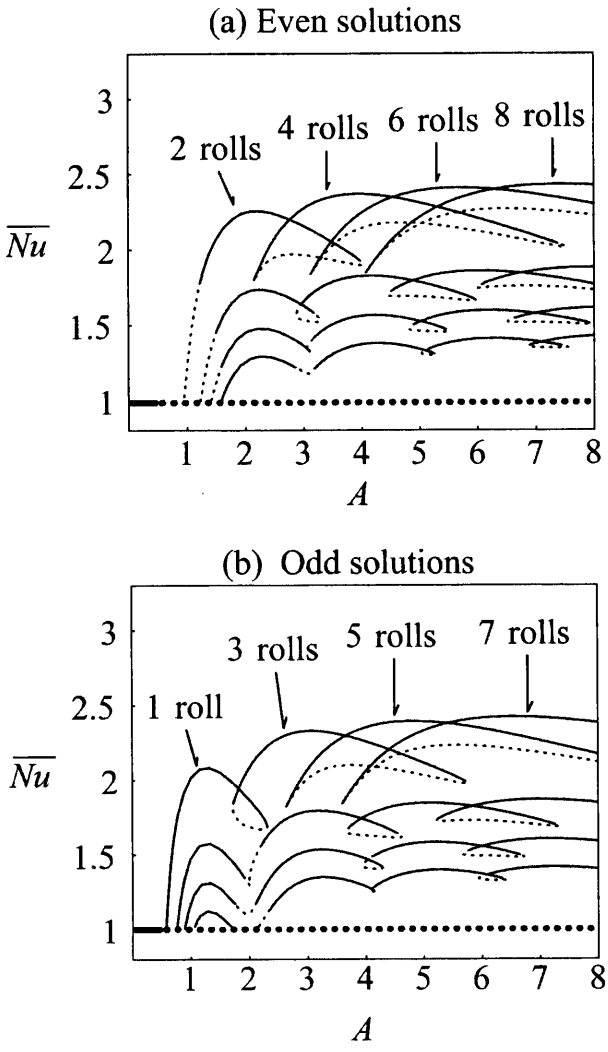

Fig. 9 First branches for perfectly insulating sidewalls. From bottom to top, $Ra = 2500$, 3000, 4000, and 8000. The solid lines denote stable solutions, and the dotted lines denote unstable solutions.

multi-valued; the branch forms a loop. The loops become larger as Ra increases.[32] In ranges of A and Ra where the loops form, n rolls and $n+2$ rolls co-exist, as we have seen in Fig. 4.

Multiple even solutions are summarized in Fig. 10(a). The solid lines represent sets of saddle-node points on the branch. We refer to Ra on the saddle-node points by R_{SN}, which depends on A. We have at least one even solution for $Ra > R_{E1}$. When $Ra > R_{SN}$, we have multiple even solutions. They represent n rolls and $n+2$ rolls in general; in some ranges of A and Ra, we have n rolls, $n+2$ rolls, and $n+4$ rolls simultaneously. If we restrict the symmetry to the odd solution only, we have a similar diagram shown in Fig. 10(b).

The solutions for the perfectly conducting sidewalls are shown in Fig. 11. Figure 12 shows neutral curves for the conducting conditions for a reference. When Ra is sufficiently higher than the critical value, the branches have folded structures with a couple of saddle-node points. The bifurcation characteristics are thus qualitatively the same as those for the perfectly insulating conditions. Note some quantitative differences here. For the conducting condition, $\overline{Nu}(A)$ is single-valued at $Ra = 2500, 3000$ and 4000 in a broad range of A. The values of R_{cusp} for the conducting condition are higher than those for the insulating condition.

We now show diagrams of linearly stable patterns in Figs. 13 and 14.[33] All of the stable patterns are provided by even and odd solutions, since the asymmetric

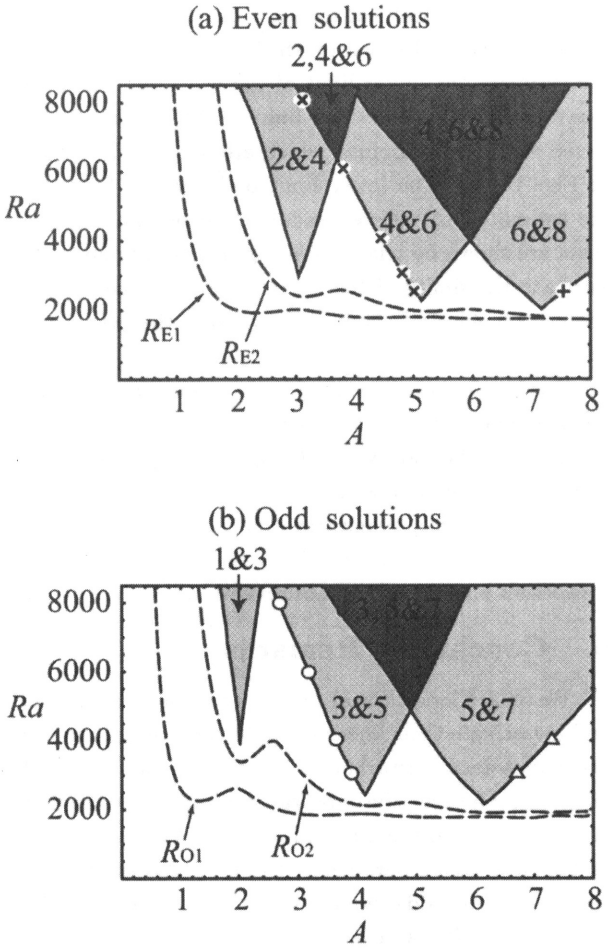

Fig. 10 Diagrams of roll solutions under assumptions on symmetry E_2 and O_1. Perfectly insulating sidewalls. The dashed lines denote the neutral Rayleigh numbers, R_{E1} and R_{E2} in (a) and R_{O1} and R_{O2} in (b). The numbers in each areas represent the numbers of rolls. For a plus, crosses, circles and triangles, see Fig. 15.

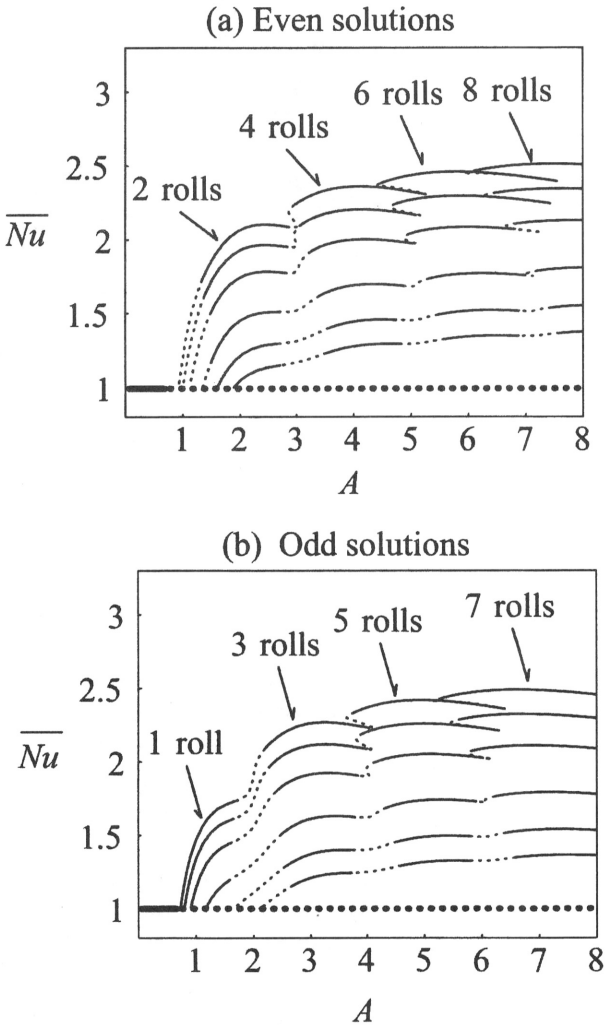

Fig. 11 First branches for perfectly conducting sidewalls. $Pr = 0.71$. From bottom to top, $Ra = 2500$, 3000, 4000, 6000, 8000, and 10000. The solid lines denote stable solutions, and the dotted lines denote unstable solutions.

solution is unstable. In these figures, the lowest two curves denote the neutral Rayleigh numbers. The lowest one, shown by the solid line, is the critical curve. The other lines represent stability boundaries of the n-roll solutions with $1 \leq n \leq 8$. Across the boundaries, even (or odd) solutions lose their stability with respect to the disturbance O_2 (or E_1).

Stable patterns depend on A and Ra. When Ra is less than R_{O1} and R_{E1}, the only stable solution is the trivial one, which corresponds to the conduction state. When Ra is greater than R_{O1} or R_{E1} for a prescribed value of A, a roll solution exists. For $R_{O1} < Ra < R_{E1}$, one odd solution is stable; see for instance $A = 1$ and $Ra = 3000$ in Fig. 13. Similarly, for $R_{E1} < Ra < R_{O1}$, one even solution exists and it is stable. For Ra above the two neutral curves R_{O1} and R_{E1}, at least one odd solution or one even solution is stable. When Ra is above the stability boundaries, additional solutions are also stable. The numbers of the rolls represented by stable solutions are listed in each areas divided by the stability boundaries. For instance, in a division including $(A, Ra) = (4, 5000)$ in Fig. 13, three solutions are stable, which represent three rolls, four rolls, and five rolls. The number of stable patterns increases as Ra increase, as far as we examined up to the eight-roll solutions.

We compare our results with previously reported results obtained by experimental and numerical studies. Goldhirsch *et al.* observed multistability of a three-roll solution and a four-roll solution based on the two-dimensional numerical simulation at $A = 3$.[34] Ouazzani *et al.* observed four rolls and sometimes three rolls in

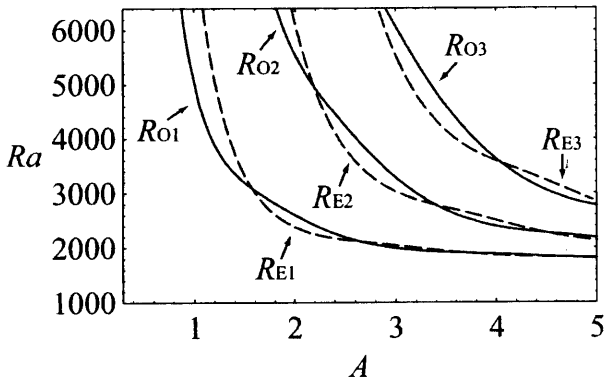

Fig. 12 Linear neutral stability curves; same as Fig. 1 but for perfectly conducting sidewalls.

their experiment at $A = 3.6$ and $Ra \leq 4700$.[35] Our results are consistent with these results. Mizushima and Adachi found that one roll is stable and two rolls are unstable at $A = 1$ and $5012 < Ra < 16624$.[21] Stability boundaries in Fig. 14 are consistent with this result, too. At $A = 4$ and $Ra = 10000$, Goldhirsch *et al.* obtained six rolls for the perfectly conducting sidewalls. On the other hand, Figs. 11 and 14 show that the stable solution consists of three, four or five rolls at $A = 4$ and $Ra = 10000$. We cannot explain this discrepancy.

Experimental supports for the diagrams in Figs. 13 and 14 have not yet been available, except for ref. 35. In a laboratory experiment, it would be difficult to change A continuously. We expect however that the stability boundaries in the diagram can be examined experimentally, by forming an appropriate roll pattern in a range (A, Ra) where multiple solutions are stable, and then decreasing Ra slowly with a fixed A. To form various roll patterns in the beginning, a technique such as the thermal imprinting[36] would be helpful.

Finally, we compare the stability boundaries for finite A to those for $A \to \infty$. Among the numerous secondary instabilities of the rolls in the infinite layer, the Eckhaus instability (sideband instability) is the only one by which a two-dimensional disturbance grows.[37] The stability boundary by the Eckhaus instability is given in terms of wave number of rolls, k. Rolls are stable for $|k - k_c| < |k_n - k_c|/\sqrt{3}$, where $k_c (= 3.116)$ is the critical wave number and k_n is the neutral wave number at a given Ra.[38]

In order to compare the present results with the Eckhaus boundary, we estimate the wave number of the rolls on the saddle-node points in Fig. 10. When A is finite, we cannot calculate the exact wave number of the rolls, because the roll patterns are not periodic in the spanwise direction. We therefore estimate the "wave number" of the rolls for finite A by $\tilde{k} = \pi/\lambda$, where λ is the width of the central roll that is closest to $x = 0$. The width is measured based on the temperature at $z = 0$. We estimate the upper limit of the wave number $\tilde{k}$ for five rolls based on the lower limit of the width λ at selected saddle-node points, which are denoted by circles in Fig. 10(b). The lower limit of $\tilde{k}$ for the five rolls are estimated at selected saddle-node points; some of them are shown by triangles in Fig. 10(b). Similarly, we estimate the limits of the wave number in the six-roll pattern on selected saddle-node points; the points are shown by a plus and crosses in Fig. 10(a).

Figure 15 shows the lower and upper limits of the wave number for five rolls and six rolls, together with the Eckhaus boundary. Although the upper limits of $\tilde{k}$ do not agree well with the Eckhaus boundary, the lower limits agree, suggesting that the Eckhaus instability mechanism may be valid even for finite A when a convection pattern consists of several rolls.

6. Concluding Remarks

We obtain longitudinal rolls in a rectangular channel and investigate their linear stability with respect to the two-dimensional disturbance. Among the first, second and third solutions, the only stable solutions are the first even solution and the first odd solution. When we use A as the bifurcation parameter, the first solution branch with even (or odd) symmetry is smooth and single-valued when Ra is close to the critical value. As Ra increases, cusps and a folded structure arise with couples of the saddle-node bifurcation points. We present diagrams of the linearly stable roll patterns in the A-Ra plane. In the present study, we use A as a bifurcation parameter and obtain bifurcation diagrams in A-$\overline{Nu}$ plane. If we use both Ra and A as bifurcation parameters, the even (or odd) solution would be expected to form a folded surface as shown in Fig. 16.

We consider only two-dimensional stability in the present paper. Even if a solution is stable with respect to two-dimensional disturbances, it can be unstable with respect to three-dimensional disturbances. That is, the stability analysis in the present study gives a necessary condition for stability. The secondary instability of the longitudinal rolls with respect to the three-dimensional disturbance has been analyzed by Clever and Busse for $A \to \infty$,[39] by Xin et al at $A = 10$,[40] and by the present authors at $A = 1, 2$,[41,42] in the presence of the throughflow. It has been confirmed that the roll solutions are stable in a certain range of parameters with respect to the three-dimensional disturbance.

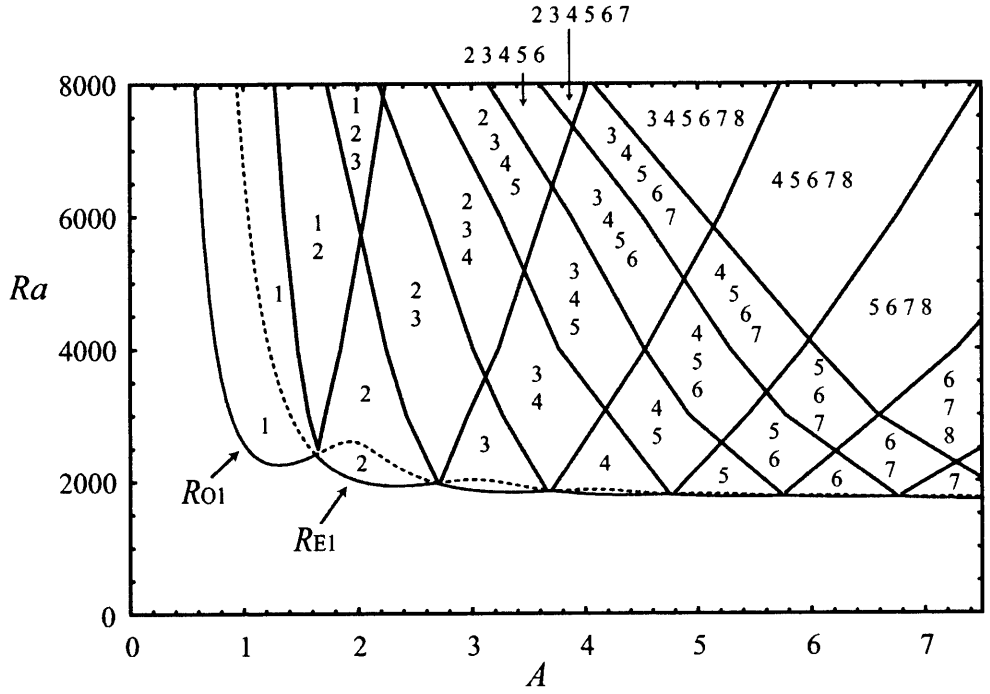

Fig. 13 Numbers of rolls in the stable solutions for perfectly insulating sidewalls. The lowest two curves denote the neutral Rayleigh numbers R_{O1} and R_{E1}; the solid one denotes critical value. All the lines, except neutral curves, represent stability boundaries of the roll solutions.

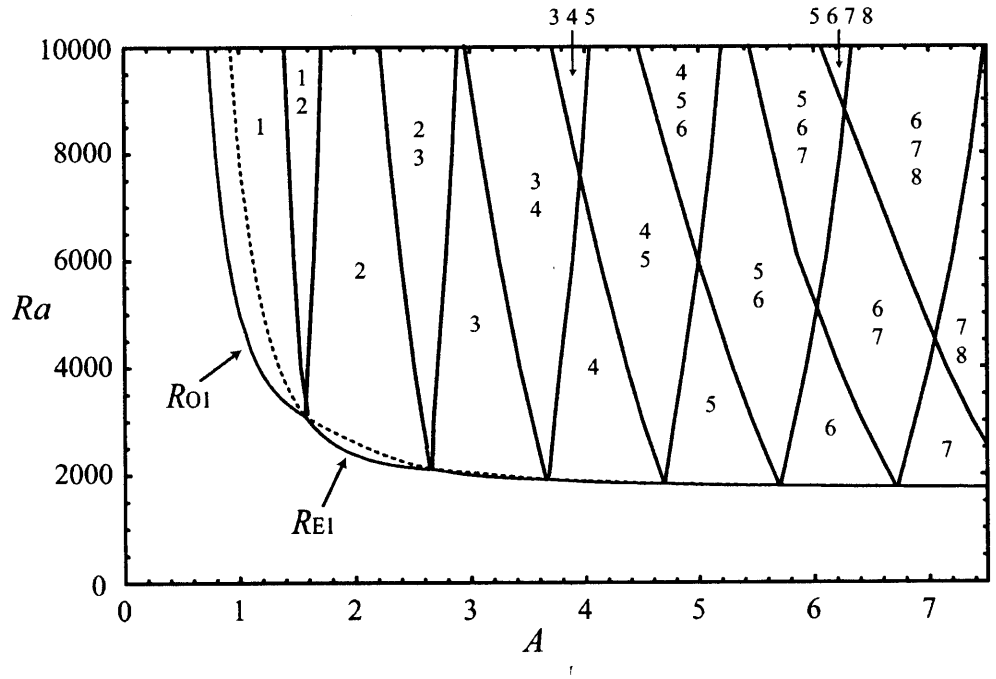

Fig. 14 Numbers of rolls in the stable solutions; same as Fig. 13 but for perfectly conducting sidewalls.

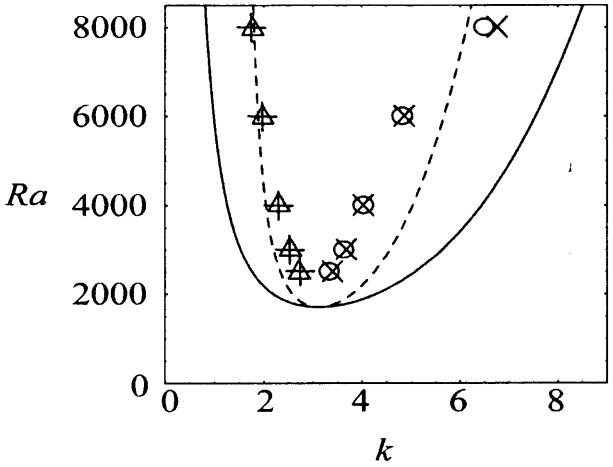

Fig. 15 Stability boundaries of five rolls and six rolls with respect to the disturbance O_1 and E_2, respectively. Perfectly insulating sidewalls. The circles and triangles denote the wave number $\tilde{k}$ for five rolls; the crosses and pluses are for six rolls. The solid line denotes the linear neutral stability curve and the dashed line denotes the Eckhaus boundary for $A \to \infty$.

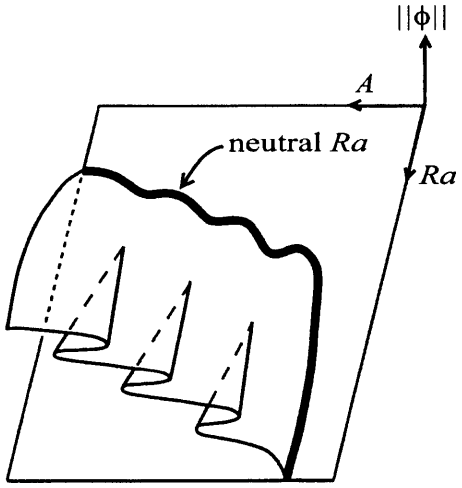

Fig. 16 A sketch of a surface formed by the even (or odd) solution. $||\phi||$ is an appropriate norm of the solution. The thick line denotes the neutral curve, which is on the A-Ra plain with $||\phi|| = 0$.

References

1) R. E. Kelly: Adv. Appl. Mech. **31** (1994) 35.

2) X. Nicolas: Int. J. Thermal Sciences **41** (2002) 961.

3) K. S. Gage and W. H. Reid: J. Fluid Mech. **33** (1968) 21.

4) K. Fujimura and R. E. Kelly: Phys. Fluids **7** (1995) 68.

5) J. K. Platten and J. C. Legros: *Convection in Liquids* (Springer, 1983) Chap. VIII, Sect. 4.

6) U. H. Kurzweg: Int. J. Heat Mass Transfer **8** (1965) 35.

7) S. H. Davis: J. Fluid Mech. **30** (1967) 465.

8) J. M. Luijkx and J. K. Platten: J. Non-Equilib. Thermodyn. **6** (1981) 141.

9) C. P. Jackson and K. H. Winters: Int. J. Numer. Methods in Fluids **4** (1984) 127.

10) B. D. Reddy and H. F. Voyé: J. Comput. Phys. **79** (1988) 92.

11) N. Y. Lee, W. W. Schultz and J. P. Boyd: Int. J. Heat Mass Transfer **32** (1989) 513.

12) J. Mizushima: J. Phys. Soc. Jpn. **64** (1995) 2420.

13) A. Y. Gelfgat: J. Comput. Phys. **156** (1999) 300.

14) X. Nicolas, J. M. Luijkx and J. K. Platten: Int. J. Heat Mass Transfer **43** (2000) 589.

15) K. A. Cliffe and K. H. Winters: J. Comput. Phys. **67** (1986) 310.

16) J. Mizushima and T. Nakamura: J. Phys. Soc. Jpn. **71** (2002) 677.

17) P. Hall and I. C. Walton: J. Fluid Mech. **90** (1979) 377.

18) H. Kidachi: Prog. Theor. Phys. **64** (1980) 1861.

19) H. Kidachi: Prog. Theor. Phys. **68** (1982) 49.

20) E. Knobloch and J. Guckenheimer: Phys. Rev. **A 27** (1983) 408.

21) J. Mizushima and T. Adachi: J. Phys. Soc. Jpn. **66** (1997) 79.

22) Y. Kato and K. Fujimura: J. Phys. Soc. Jpn. **75** (2006) 034401.

23) Y. Kato: RIMS Kokyuroku Bessatsu **B3** (2007) 25.

24) T. B. Benjamin: Proc. R. Soc. Lond. **A359** (1978) 27.

25) T. Mullin: J. Fluid Mech. **121** (1982) 207.

26) D. G. Scheaffer: Math. Proc. Camb. Phil. Soc. **87** (1980) 307.

27) P. Hall: Proc. R. Soc. Lond. **A384** (1982) 359.

28) L. Fung, K. Nandakumar and J. H. Masliyah: J. Fluid Mech. **177** (1987) 339.

29) J. Yamada, T. Miyazaki and I. Hosokawa: J. Jpn. Soc. Fluid Mech. **15** (1996) 417 (in Japanese).

30) Y. Kato and K. Fujimura: Phys. Rev. E **62** (2000) 601.

31) H. B. Keller: *Applications of bifurcation theory* (Academic Press, 1977) 359.

32) In Fig. 9, the solution branch at $Ra = 8000$ may look to have couples of sharp cusps along loops. They are spurious cusps; they are saddle-node bifurcation points.

33) To obtain diagrams in Figs. 13 and 14, we use the secondary instability analyses explained in §2.3 and the neutral conditions of the conduction state in ref. 12. We first estimated the boundaries based on the secondary instability analyses at selected values of Ra, which are $Ra = 2500, 3000, 4000, 6000$ and 8000 for the insulating condition. For the conducting condition, results at $Ra = 10000$ are added. We have not examined the stability of the roll for $Ra < 2500$. To draw the stability boundaries in this range, we connect two points: the point at which the stability changes at $Ra = 2500$ and the crossover points of two neutral curves. Here, the crossover point is the point at which $R_{O1} = R_{E1}$ holds. The aspect ratios and Rayleigh numbers at the crossover points are listed in ref. 12.

34) I. Goldhirsch, R. B. Pelz and S. A. Orszag: J. Fluid Mech. **199** (1989) 1.

35) M. T. Ouazzani, J. K. Platten and A. Mojitabi: Int. J. Heat Mass Transfer **33** (1990) 1417.

36) M. M. Chen and J. A. Whitehead: J. Fluid Mech. **31** (1968) 1.

37) R. M. Clever and F. H. Busse: J. Fluid Mech. **65** (1974) 625.

38) W. Eckhaus: *Studies in nonlinear stability theory* (Springer, 1965). Chap. 8.

39) R. M. Clever and F. H. Busse: J. Fluid Mech. **229** (1991) 517.

40) S. Xin, X. Nicolas and P. Le Quéré: Numerical Heat Transfer, Part A, Vol. 50, (2006) 467.

41) Y. Kato and K. Fujimura: Theoretical and Applied Mechanics **50** (2001) 327.

42) Y. Kato: Reports of Research Institute for Applied Mechanics, Kyushu Univ, **139** (2010) 31.